CHEMISTRY OF MATERIALS
Article

Chem. Mater. **2010,** *22,* 1821–1830 1821
DOI:10.1021/cm9033484

Advanced Drug Delivery Vectors with Tailored Surface Properties Made of Mesoporous Binary Oxides Submicronic Spheres

Montserrat Colilla,[†,‡] Miguel Manzano,[†,‡] Isabel Izquierdo-Barba,[†,‡] María Vallet-Regí,*[,†,‡] Cédric Boissiére,[§] and Clément Sanchez[§]

[†]*Dpto Química Inorgánica y Bioinorgánica, Facultad de Farmacia, Universidad Complutense de Madrid, Plaza Ramón y Cajal s/n, 28040 Madrid, Spain,* [‡]*Networking Research Center on Bioengineering, Biomaterials and Nanomedicine (CIBER-BBN), Madrid, Spain, and* [§]*CNRS, UPMC University of Paris 06, UMR 7574, Laboratoire Chimie de la Matière Condensée de Paris, Paris F-75005, France*

Received November 2, 2009. Revised Manuscript Received December 9, 2009

The synthesis of mesoporous silica-zirconia mixed oxides that can be used as efficient drug delivery carriers for bisphosphonates based drugs has been performed via spray-drying process. These silica-zirconia mixed oxides used for the first time as drug delivery systems exhibit mesostructures with tunable acidity. The two selected drugs were alendronate and zoledronate, which carry similar phosphonate heads but different amine tails in terms of acidity and hydrophobicity. The incorporation of different zirconium amounts into the mesostructured silica network creates Lewis and Brönsted acid surface sites allowing to control the surface properties of the mesoporous matrix and therefore the amount of phosphonate adsorbed into the mesopores. This effect occurs even at low ZrO_2 contents and produces a noticeable modification on the release behavior of bisphosphonates. The partial retention of the drug through phosphonates complexation by zirconium sites leads to a more sustained release of the drug. These binary ordered mesoporous oxides act as versatile controlled release vectors of bisphosphonates with potential application in bone implant technologies. This novel application of these silica-zirconia oxides and their capability to tune the drug release kinetics augur a significant advance in the field of materials science.

Introduction

The mushrooming expansion of nanotechnologies has recently motivated the research on new nanostructured materials for biomedical applications.[1−5] One important biomedical development concerns the research of porous materials eligible for loading and releasing drugs or biologically active molecules in a controlled manner.[6,7] Indeed, controlled drug-delivery systems are one of the most promising applications for human health care.[8] A smart drug delivery carrier should be able to target specific zones of the body and to control the rate and period of drug delivery. Mesoporous silica based materials are characterized by high surface areas, important pore volumes, periodically ordered network of monodisperse pore with controlled pore size, texture and surface functionalization, allowing a high loading of active molecules and fine control of release kinetics.[4,9] Therefore, these versatile hosts have been proposed as implantable, oral, transdermal, injectable drug reservoirs, and for bone tissue regeneration.[1,9,10]

Moreover, out looking toward the future, silica based mesoporous matrices will probably contribute to the development of new carriers with sophisticated stimuli-response capability[10−14] and multifunctional platforms that allow targeting, diagnosis, and multiple therapies.[15−17] However, at present, one of the main and more specific problems of drug delivery vectors is the loss of activity of some drugs before reaching the target as a result of premature degradation of the carrier or of the active agent. In this

*Corresponding author e-mail: vallet@farm.ucm.es.

(1) Vallet-Regí, M. *Chem.—Eur. J.* **2006**, *12*, 5934–5943.
(2) Vallet-Regí, M.; Ruiz-González, L.; Izquierdo-Barba, I.; González-Calbet, J. M. *J. Mater. Chem.* **2006**, *16*, 26–31.
(3) Goldberg, M.; Langer, R.; Jia, X. Q. *J. Biomater. Sci., Polym. Ed.* **2007**, *18*, 241–268.
(4) Vallet-Regí, M.; Balas, F.; Arcos, D. *Angew. Chem., Int. Ed.* **2007**, *46*, 7548–7558.
(5) Webster, T. J.; Ahn, E. S. *Adv. Biochem. Eng. Biotechnol.* **2007**, *103*, 275–308.
(6) Vallet-Regí, M.; Rámila, A.; Del Real, R. P.; Pérez-Pariente, J. *Chem. Mater.* **2001**, *13*, 308–311.
(7) Vallet-Regí, M. *Key Eng. Mater.* **2008**, *377*, 1–18.
(8) Langer, R. *Science* **1990**, *249*, 1527–1533.
(9) Vallet-Regí, M.; Colilla, M.; Izquierdo-Barba, I. *J. Biomed. Nanotechnol.* **2008**, *4*, 1–15.
(10) Giri, S.; Trewyn, B. G.; Stellmaker, M. P.; Lin, V.S.-Y. *Angew. Chem., Int. Ed.* **2005**, *44*, 5038–5044.
(11) Chang, H.; Shim, C. H.; Kim, B. J.; Shin, Y.; Exarhos, G. J.; Kim, K. *J. Adv. Mater.* **2005**, *17*, 634–637.
(12) Lai, C. Y.; Trewyn, B. G.; Jeftinija, D. M.; Jeftinija, K.; Xu, S.; Jeftinija, S.; Lin, V.S.-Y. *J. Am. Chem. Soc.* **2003**, *125*, 4451–4459.
(13) Hernández, R.; Tseng, H. R.; Wong, J. W.; Stoddart, J. F.; Zink, J. I. *J. Am. Chem. Soc.* **2004**, *126*, 3370–3371.
(14) Slowing, I. I.; Trewyn, B. G.; Giri, S.; Lin, V.S.-Y. *Adv. Funct. Mater.* **2007**, *17*, 1225–1236.
(15) Ruiz-Hernández, E.; López, A.; Arcos, D.; Izquierdo-Barba, I.; Terasaki, O.; Vallet-Regí, M. *Chem. Mater.* **2007**, *19*, 3455–3463.
(16) Ruiz-Hernández, E.; López-Noriega, A.; Arcos, D.; Vallet-Regí, M. *Solid State Sci.* **2008**, *10*, 421–426.
(17) Julián-López, B.; Boissière, C.; Chanéac, C.; Grosso, D.; Vasseur, S.; Miraux, S.; Duguet, E.; Sanchez, C. *J. Mater. Chem.* **2007**, *17*, 1563–1569.

Published on Web 12/31/2009

sense, the employment of mesoporous silica particles as host matrices of different guest molecules to be locally delivered in the place where needed once implanted offers certain benefits in bone implant technologies. Moreover, it has been demonstrated that different molecules preserve their activity when confined into mesoporous silica frameworks.[18,19]

Recently, the dynamic behavior of nanoscale mesoporous silica based thin films exposed to biologically relevant conditions has been shown to be highly dependent on composition, porosity, and calcination temperature. While pure mesoporous silica thin films underwent a rapid degradation, occurring on the time scale of hours, silica-zirconia mesoporous films were significantly more stable making them relevant for the culture and growth of cells and for drug release applications.[20] From the standpoint of drug delivery, the presence of zirconia is interesting since it could provide the opportunity to tailor the controlled capture and release of bioactive molecules based on metal complexation.

Bisphosphonates are the most widely used drugs for the treatment of osteoporosis, Paget's disease, and tumor-related diseases.[21] They are synthetic analogues of the endogenous mineral deposition inhibitor pyrophosphate, which is the natural modulator of bone metabolism. These bisphosphonates have been shown to inhibit the osteoclasts resorption of bone tissue, but they present a low intestinal absorption and a highly selective location and retention in bone.[22] Those two characteristics make necessary the oral administration of really high doses with the subsequent gastrointestinal and renal problems for the patients. To overtake these side effects, bisphosphonates could be introduced into implantable devices that would enable a local and controlled drug delivery. Thus, different matrices have been proposed as local controlled delivery systems of bisphosphonates.[23−26] Recently, it has been reported that the incorporation of bisphosphonates into the pores of mesostructured silicas may inhibit bone resorption at local level once implanted in osteoporotic bone.[27−29] In this sense, ordered mesoporous matrices are promising candidates for the design of bisphosphonates controlled delivery devices.

This article describes the synthesis of mesoporous silica-zirconia mixed oxides that can be used as efficient local drug delivery devices. The novelty of this research work is based on the employment of Zr-containing mesoporous silicas as bisphosphonates release systems. It should be highlighted the delay and/or retention of the drug found during the in vitro release tests. The synthesis uses a very attractive spray-drying process that limits the number of synthesis steps.[30−32] After atomization, the microdroplets are dried within the carrying gas which induces the progressive concentration in nonvolatile species allowing the polymer micelle self-assembly to occur while condensation of the two inorganic precursors takes place. The final mesostructured particles are then calcined to obtain the mesoporous particles.[33] Most importantly, the two step synthesis procedure presented allows the precise control of Zr/Si molar ratios from 0% to 20% since the Si/Zr ratio fixed in the initial solution is preserved in the powder. The spray-drying process is furthermore advantageous compared to the precipitation based approaches because it not only authorizes via a kinetic quench the formation of structures with new compositions but it can also be easily scaled up as an industrial viable continuous and fast process.

The structure and properties of these materials have been thoroughly characterized by X-ray diffraction (XRD), X-ray fluorescence (XRF), transmission electronic microscopy (TEM), Fourier transform infrared spectroscopy (FTIR), nitrogen adsorption−desorption isotherms, and zeta potential (ζ) measurements. The release kinetics of two phosphonates based drugs zoledronate and alendronate have been studied following previously validated procedures of high performance liquid chromatography (HPLC).[34,35] These SiO_2-ZrO_2 mixed oxides used for the first time as drug delivery systems exhibit periodic large pore mesostructures with tunable acidity. Moreover the possibility of adjusting the control release of certain drugs by varying the composition of mesostructured binary oxides is demonstrated. The uptake and release of the drugs can finely be tuned by adjusting the pH loading and the complexing capacity of the surface that depends on the zirconia content.

Materials and Methods

Synthesis of Materials. The synthesis of mesoporous silica particles loaded with Zr was carried out by evaporation induced

(18) Deere, J.; Magner, E.; Wall, J. G.; Hodnett, B. K. *J. Phys. Chem. B* **2002**, *106*, 7340–7347.
(19) Hartmann, M. *Chem. Mater.* **2005**, *17*, 4577–4593.
(20) Bass, J. D.; Grosso, D.; Boissiere, C.; Belamie, E.; Coradin, T.; Sanchez, C. *Chem. Mater.* **2007**, *19*, 4349–4356.
(21) Rodan, G. A.; Martin, T. J. *Science* **2000**, *289*, 1508–1514.
(22) Russell, R. G. G.; Rogers, M. J. *Bone* **1999**, *25*, 97–106.
(23) Patashnik, S.; Rabinovich, L.; Golomb, G. J. *Drug Target* **1997**, *4*, 371–380.
(24) Josse, S.; Faucheux, C.; Soueidan, A.; Grimandi, G.; Massiot, D.; Alonso, B.; Janvier, P.; Laïb, S.; Pilet, P.; Gauthier, O.; Daculsi, G.; Guicheux, J.; Bujoli, B.; Bouler, J. M. *Biomaterials* **2005**, *26*, 2073–2080.
(25) Seshima, H.; Yoshinari, M.; Takemoto, S.; Hattori, M.; Kawada, E.; Inoue, T.; Oda, Y. *J. Biomed. Mater. Res. Part B* **2006**, *78B*, 215–221.
(26) Roussiere, H.; Fayon, F.; Alonso, B.; Rouillon, T.; Schnitzler, V.; Verron, E.; Guicheux, J.; Petit, M.; Massiot, D.; Janvier, P.; Bouler, J. M.; Bujoli, B. *Chem. Mater.* **2008**, *20*, 182–191.
(27) Balas, F.; Manzano, M.; Horcajada, P.; Vallet-Regí, M. *J. Am. Chem. Soc.* **2006**, *128*, 8116–8117.
(28) Nieto, A.; Balas, F.; Colilla, M.; Manzano, M.; Vallet-Regí, M. *Microporous Mesoporous Mater.* **2008**, *116*, 4–13.
(29) Shi, X. T.; Wang, Y. J.; Varshney, R. R.; Ren, L.; Zhang, F.; Wang, D. A. *Biomaterials* **2009**, *30*, 23–24.
(30) Bruinsma, P. J.; Kim, A. Y.; Liu, J.; Baskaran, S. *Chem. Mater.* **1997**, *9*, 2507–2512.
(31) Brinker, C. J.; Lu, Y.; Sellinger, A.; Fan, H. *Adv. Mater.* **1999**, *11*, 579–585.
(32) Grosso, D.; Soler-Illia, G. J. A. A.; Crepaldi, E. L.; Sanchez, C. *Adv. Funct. Mater.* **2003**, *13*, 37–42.
(33) Baccile, N.; Grosso, D.; Sanchez, C. *J. Mater. Chem.* **2003**, *13*, 3011–3016.
(34) De Marco, J.; Biffar, S. E.; Reed, D. G.; Brooks, M. A. *J. Pharm. Biomed. Anal.* **1989**, *7*, 1719–1727.
(35) Rao, B. M.; Srinivasu, M. K.; Rani, C. P.; Kumar, S. S.; Kumar, P. R.; Chandrasekhar, K. B.; Veerender, M. *J. Pharm. Biomed. Anal.* **2005**, *39*, 781–790.

Table 1. Different Molar Compositions of the Sols Produced

sample	F127	Si	Zr	EtOH	H_2O
FSZ_0	0.005	1	-	20	20
$FSZ_{3.5}$	0.005	0.965	0.035	20	20
FSZ_7	0.005	0.93	0.07	20	20
FSZ_{10}	0.005	0.9	0.1	20	20
FSZ_{20}	0.005	0.8	0.2	20	20

self-assembly (EISA) method using an aerosol route.[31] The synthesis is based on the use of the nonionic surfactant F127 ($(EO)_{106}(PO)_{70}(EO)_{106}$) as structure directing agent, which was dissolved in a mixture of ethanol and water. Then, zirconium tetrachloride and tetraethyl orthosilicate were added in different proportions to obtain sols with diverse molar compositions (see Table 1). An aerosol process[31] was applied to these sols to produce the SiO_2-ZrO_2 mesoporous particles: compressed air drew the sol into an atomizer, which produced the aerosol droplets that were carried through a glass tube heated at 400 °C. At this temperature the solvent evaporation from the aerosol droplets promoted the self-assembly of surfactant and oxides into ordered mesostructures. The produced particles were then collected into a filter placed at the end of the glass tube. The surfactant was then removed through 2 consecutive thermal cycles at 550 °C for 16 h with a heating rate of 5 °C/min under nitrogen (first 2 h) and oxygen atmosphere. The effective removal of the surfactant was confirmed by thermal analyses (thermogravimetric (TG) and differential thermal analysis (DTA)).

Characterization of Materials. The synthesized materials were characterized using TEM with a JEOL 3000 FEG electron microscope fitted with a double tilting goniometer stage (±45°) and with an Oxford LINK EDS analyzer. TEM images were recorded using a CCD camera (MultiScan model 794, Gatan, 1024 × 1024 pixels, size 24 μm × 24 μm) using low-dose condition. FT patterns were conducted using Digital Micrograph (Gatan). energy dispersive spectrometry (EDS) analyses were performed with an Oxford model ISIS. XRD measurements were performed in a Philips X′pert diffractometer over the range of 0.5° and 5° of 2θ using Cu Kα radiation at 1.5418 Å), FTIR (Nicolet Nexus spectrometer using the KBr pellet method), and elemental analysis (Perkin-Elmer 2400 CHN analyzer). TG and DTA thermal analyses were carried out in dynamic oxygen atmosphere between 40 and 800 °C (air flow rate of 100 mL min^{-1}) using a Perkin-Elmer Diamond analyzer. The surface characterization of materials was carried out by N_2 adsorption/desorption analysis at −196 °C on a Micromeritics ASAP 2020 analyzer. Before measurements, the samples were outgassed under vacuum for 24 h at 200 °C. The BET equation was used to calculate the surface area S_{BET} from adsorption data obtained at P/P_0 between 0.05 and 0.2. The total volume of pores, V_P, was calculated from the amount of the N_2 adsorbed at $P/P_0 = 0.97$, assuming that adsorption on the external surface was negligible compared to adsorption in pores. The average mesopore size (D_P) was obtained from the maximum of the pore size distribution calculated from the adsorption branch of the isotherm by means of the Barrett−Joyner−Halenda (BJH) method.[36] To assess the possible existence of micropores (pore diameter < 2 nm) in samples, the t-plot method was employed.

The ζ-potential measurements were performed in a Zetasizer Nano Series instrument coupled to a MPT-2 multipurpose titrator from Malvern. ζ-potential can be described by Smoluchowski's equation:[37] $\zeta = 4\pi\eta\ U/\varepsilon$, where U is the electrophoretic mobility, η is the viscosity of water, and ε is the dielectric constant of water. Five milligrams of each powdered sample was added to 10 mL of KCl 10 mM (used as the supporting electrolyte); the pH was adjusted by adding appropriate volumes of 0.10 M HCl or 0.10 M KOH solutions.

Bisphosphonates Loading. Sodium alendronate trihydrate was kindly supplied by Merck-Sharp-Donne Co. Inc. MSD, New Jersey, USA. Drug adsorption was performed following previously described procedures[27,28] by soaking 100 mg portions of the powders in 5 mL of a buffered aqueous solution of sodium alendronate (62 mM) at pH 4.8 (CH_3COO^-/CH_3COOH buffer, 50 mM) for 24 h at room temperature. Zoledronate (kindly supplied by Novartis) adsorption was carried out by soaking 400 mg of each powered material in 4 mL of an aqueous zoledronate (20 mg/mL) solution for 24 h magnetically stirring at room temperature. Then, both, alendronate and zoledronate loaded materials were dried in a vacuum oven at 37 °C for 7 days. After this, pieces of 50 mg of each mesoporous material were prepared using uniaxial and isostatic pressure to obtain disks of 6 mm of diameter. Three pieces of each loaded material at pH 4.8 for alendronate and at pH 3.5 zoledronate were prepared to secure reproducibility during the release experiments. The drug loading was determined using XRF, a method commonly reported in the literature for the quantification of bisphosphonates.[27,28]

Bisphosphonates Release. The alendronate delivery assays were carried out by soaking three 50 mg pieces of each material in a NaCl 0.9% saline solution at 37 °C and physiological pH of 7.4 (the pH was buffered using a 50 mM aqueous solution of tris(hydroxymethyl)aminomethane). 0.9% NaCl saline solution was chosen as the release medium because it is the simplest simulated body fluid, so the possible different behavior of the materials could be unquestionably assigned to the materials themselves, rather than to the delivery medium. Continuous magnetic stirring was applied during the delivery tests. The alendronate released was quantified by RP-HPLC in a Waters Alliance automatic analysis system composed by a Model#2695 separations module coupled to a Model#2996 photodiode array detector and controlled by the software Millenium_32. The RP-HPLC procedure for the determination of NaAL implies the precolumn derivatization with 9-fluorenylmethyl cloroformate (FMOC, 97%, Aldrich).[34] Chromatographic separations were carried out with a 250 × 4.6 mm prepacked analytical column Mediterranea Sea18 (Teknokroma Inc.; Spain) containing 5 μm C-18 functionalized silica beads. The isocratic mobile phase was a mixture of 25 mM sodium citrate and potassium phosphate mixture at pH 8.0, acetonitrile, and methanol (75:20:5, v/v) at 0.8 mL/min at 310 K. The injection volume was 10 μL, and detection was performed by UV at 266 nm. Under these conditions, the retention time of NaAL−FMOC was 8.0 ± 0.5 min.

The zoledronate delivery experiments were carried out by soaking three 50 mg pieces of each material, FSZ_0, $FSZ_{3.5}$, FSZ_7, FSZ_{10}, and FSZ_{20}, in a NaCl 0.9% saline solution at 37 °C and physiological pH of 7.4 (the pH was buffered using a 50 mM aqueous solution of tris(hydroxymethyl)aminomethane). Continuous magnetic stirring was applied during the delivery tests. The zoledronate released was quantified by reverse phase RP-HPLC in a Waters Alliance automatic analysis system. The RP-HPLC procedure for the determination of zoledronate[35] was carried out using a Waters x Terra RP18, 250 mm x 4.6 mm, 5 μm column using a mobile phase containing a mixture of aqueous 8 mM dipotassium hydrogen orthophosphate, 2 mM

(36) Barrett, E. P.; Joyner, L. G.; Halenda, P. H. *J. Am. Chem. Soc.* **1951**, *73*, 373–381.
(37) Smoluchowski, M. V. In *Handbuch der Electrizitat und des Magnetismus*; Barth, Ed.; Leipzig, Germany, 1921; p 366.

disodium hydrogen orthophosphate, and 7 nM tetra-n-butyl ammonium hydrogen sulfate and methanol (95:5, v/v). The flow rate of the mobile phase was 0.7 mL min^{-1}, the injection volume was 10 μL, the column temperature was maintained at 25 °C, and the wavelength was monitored at 215 nm.

Results and Discussion

Characterization of Materials. Mesostructured ordered binary oxides in the SiO_2-ZrO_2 system have been investigated here for the first time as drug delivery systems. The synthesis of these mesostructured matrices composed of silica and zirconia was based on the EISA method[30] using an aerosol route. This method permits the synthesis of materials whose compositions are thermodynamically out of the scope of the traditional precipitation methods.[38] Pluronic F127 was used as structure directing agent to yield 3D-cubic cage-type ($Im\bar{3}m$ space group) mesostructures with different Si/Zr molar ratios. The resulting mesostructured materials are designated FSZ_x, where F stands for the surfactant used F127, S for silica, Z for zirconia, and x for the amount of zirconia precursor present in the nominal composition of each material (Table 1).

The morphology of the produced particles was evaluated using scanning electron microscopy (SEM) (data not shown) and also by TEM studies as discussed below. As expected, spherical particles with heterogeneous particle diameter distribution were obtained. The spherical morphology is a consequence of the synthetic process employed, where the initial solution of silica and zirconia precursors together with the surfactant are diluted in a mixture of ethanol and water. Using the aerosol, spherical droplets of this solution are passed through a tubular oven where the particles are dried with preferential alcohol evaporation which induces the micelle formation and the subsequent mesophase formation.[39,40] At the end of the process, well-ordered spherical particles with stable pore mesostructure were obtained.

The structural characterization of mesoporous silica spheres with different ZrO_2 content has been performed by powder XRD and TEM. Figure 1 shows powder XRD corresponding to silica based mesoporous spheres as function of ZrO_2 content. All materials display XRD patterns with two well-resolved peaks which could be indexed as 110 and 211 of cubic phase by assuming the observation of some domain of a body-centered cubic structure ($Im\bar{3}m$, space group) by TEM studies.[41,42] Only in the case of FSZ_{10} sample one well-resolved peak and two weak shoulders are observed, which can be indexed as 110, 200, and 211 reflections, respectively, which could indicate a higher rate of ordered arrangement in such sample. Moreover, a decrease of unit cell parameter is observed as function of ZrO_2 content from a value 19.5 to 11.8 nm corresponding to FSZ_0 and FSZ_{20} samples, respectively (see Table 2). Low magnification TEM images (Figure 2a and 2c) show heterogeneity in particle size in the 100−400 nm range in all samples. Higher magnifications TEM micrographs (Figure 2b and 2d) show mesostructures arrangement wormlike-type. Fourier transform (FT) diffractograms were obtained from the digitized TEM images (Figure 2e and 2f), where very diffuse reflections are observed. Then by placing a small window around these reflections in the FT, a subsequent inverse Fourier transformation strongly suppress high-frequency nonperiodic noise from the image. The obtained Fourier-filtered images (Figure 2g and 2h) clearly show different areas which follow an ordered mesoporous arrangement with body centered cubic structure $Im\bar{3}m$ space group.[41]

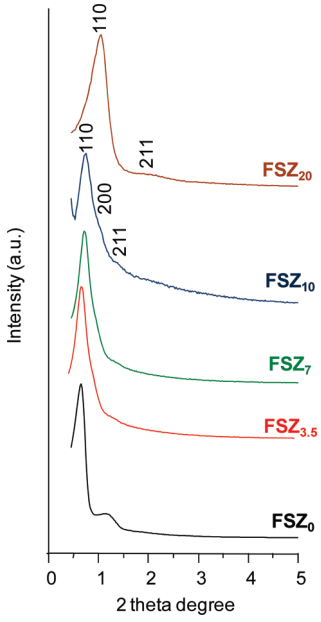

Figure 1. XRD patterns of mesoporous silica spheres with different ZrO_2 contents.

Table 2. Characteristics of FSZ_x Samples Obtained from N_2 Adsorption Isotherms, XRD, and ζ-Potential Measurements[a]

sample	S_{BET} (m^2/g)	V_P (cm^3/g)	$V_{\mu m}$ (cm^3/g)	D_P (nm)	a_0 (nm)	t_{wall} (nm)	IEP
FSZ_0	376	0.78	0.0245	11.0	19.5	5.9	1.9
$FSZ_{3.5}$	379	0.43	0.0536	8.4	17.6	6.8	1.0
FSZ_7	390	0.45	0.0638	8.4	17.3	6.6	0.6
FSZ_{10}	375	0.38	0.0530	8.0	16.4	6.2	0.4
FSZ_{20}	275	0.23	0.0334	4.6	11.8	5.6	0.4

[a] S_{BET} is the surface area determined by using the BET method between the relative pressures (p/p_0) 0.05−0.25. V_P and $V_{\mu P}$ are, respectively, the total pore volume and micropore volume obtained using the t-plot method. The total pore volume was estimated from the amount adsorbed at a relative pressure of 0.99. [c] D_P is the pore diameter calculated by means of the BJH method from the adsorption branch of the isotherm. a_0 is the unit cell parameter calculated by XRD, being $a_0 = d_{110} \cdot \sqrt{2}$. t_{wall} is the wall thickness calculated using the equation $t_{wall} = a_0 \cdot (\sqrt{3}/2) - D_P$ for cubic $Im\bar{3}m$ structures.[59] IEP is the isoelectric point obtained from ζ-potential measurements.

(38) Grosso, D.; Cagnol, F.; Soler-Illia, G.; Crepaldi, E. L.; Amenitsch, H.; Brunet-Bruneau, A.; Bourgeois, A.; Sanchez, C. *Adv. Funct. Mater.* **2004**, *14*, 309–322.
(39) Lu, Y. F.; Fan, H. Y.; Stump, A.; Ward, T. L.; Rieker, T.; Brinker, C. J. *Nature* **1999**, *398*, 223–226.
(40) Boissiere, C.; Grosso, D.; Amenitsch, H.; Gibaud, A.; Coupé, A.; Baccile, N.; Sanchez, C. *Chem. Commun.* **2003**, 2798–2799.
(41) Sakamoto, Y.; Kaneda, M.; Terasaki, O.; Zhao, D. Y.; Kim, J. M.; Stucky, G.; Shim, H. J.; Ryoo, R. *Nature* **2000**, *408*, 449–453.
(42) García-Bennett, A. E.; Kupferschmidt, N.; Sakamoto, Y.; Che, S.; Terasaki, O. *Angew. Chem., Int. Ed.* **2005**, *44*, 5317–5322.

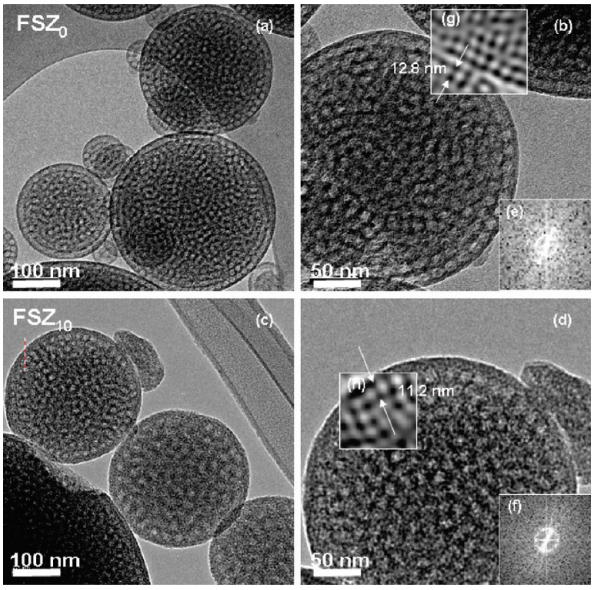

Figure 2. Electron microscopy study corresponding to the mesoporous silica spheres with 0 and 10% (% wt) of ZrO_2, respectively (FSZ_0 and FSZ_{10} samples). (a, c) Low magnification TEM image showing different size of spheres particles in both systems, (b, d) higher magnification of TEM images, (e, f) corresponding FT diffraction patterns, and (g, h) filtered TEM images. Small domains correlating to the [100] direction of a body centered cubic cage-type structure with a $Im\bar{3}m$ space group are shown in the filtered TEM images.

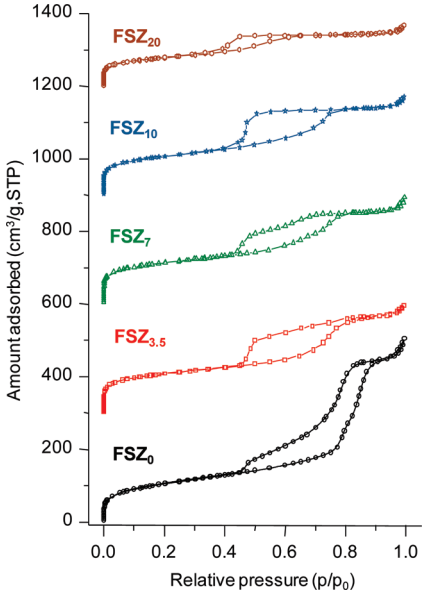

Figure 3. N_2 adsorption isotherms of FSZ_x materials, where $x = 0$, 3.5, 7, 10, and 20. The N_2 adsorption isotherms for samples $FSZ_{3.5}$, FSZ_7, FSZ_{10}, and FSZ_{20} were vertically offset by 300, 600, 900, and 1200 cm^3/g STP, respectively.

The chemical composition corresponding to these samples have been performed by EDS coupled to TEM microscope, analyzing a number of ten spheres of each sample (see Table 3). These results, which are in good agreement with those determined by XRF, show the homogeneous distribution of silicon and zirconium in spheres studied in the ratio Si/Zr expected.

Porosities of the produced binary oxides were characterized by N_2 adsorption−desorption experiments (Figure 3). In all cases, and independently of the amount of zirconia present, all the samples display distinctive type-IV isotherms typical of mesoporous materials. Moreover, the desorption branches of the N_2 isotherms do not line the adsorption branches, leading to adsorption−desorption hysteresis loops. Two different components can be observed in such hysteresis loops; the first one could be attributed to H2 hysteresis loop characteristic of cagelike mesopores.[43] The second component of the hysteresis loop could be ascribed to wormlike-type mesoporous arrangements. These findings would be in good agreement with the results derived from TEM studies, which pointed to the existence of wormlike-type arrangements of mesopores with body centered cubic structure ($Im\bar{3}m$ space group) domains.

Table 2 summarizes the different textural properties of FSZ_x samples derived from the treatment of N_2 adsorption and XRD data. Generally, the textural properties of FSZ_x samples decrease as the ZrO_2 content rises. However, data shown in Table 2 reveal that there are only slight variations in the BET surface areas of FSZ_x materials for $x \leq 10$, which do not follow any significant trend. These S_{BET} values remain in the 375−390 m^2/g range in all cases independently of the ZrO_2 content. However, the S_{BET} value of the sample with the highest ZrO_2 content experiences a remarkable decrease to 275 m^2/g, which should strongly influence bisphosphonates adsorption and release behaviors. This decrease in the surface area could be ascribed to the great extent of the density of the samples as Zr atoms replace Si ones in mixed oxides.[44]

This fact is consistent with previous observations in which the effective incorporation of heteroelements into the silica walls led to a decrease in the surface area and pore diameter.[45−49] The pore volume (V_P) values gradually and drastically decrease as the ZrO_2 content increases in FSZ_x samples. However, the micropore volume ($V_{\mu P}$) increases in SiO_2−ZrO_2 mixed oxides compared to pure silica mesoporous material (FSZ_0), in agreement with previous research works.[46] Moreover, the main pore diameter (D_P) decreases as the ZrO_2 content in FSZ_x samples raises, ranging from 11.0 nm for FSZ_0 to 8.0 nm for FSZ_{10} materials. The sample with the highest Zr content (FSZ_{20}) presents a very small D_P of 4.6 nm. N_2 adsorption data combined with XRD data (a_0) also permits to calculate the wall thicknesses (t_{wall}) of the mesoporous walls, as displayed in Table 2. The results

(43) Morishige, K.; Tateishi, N.; Fukuma, S. J. *Phys. Chem. B* **2003**, *107*, 5177–5181.
(44) de Zarate, D. O.; Gomez-Moratalla, A.; Guillem, C.; Beltran, A.; Latorre, J.; Beltran, D.; Amoros, P. *Eur. J. Inorg. Chem.* **2006**, 2572–2581.
(45) Pirard, R.; Bonhomme, D.; Kolibos, S.; Pirard, J. P.; Lecloux, A. *J. Sol-Gel Sci. Technol.* **1997**, *8*, 831–836.
(46) Tarafdar, A.; Panda, A. B.; Pramanik, P. *Microporous Mesoporous Mater.* **2005**, *84*, 223–228.
(47) Tuel, A. *Microporous Mesoporous Mater.* **1999**, *27*, 151–169.
(48) Colilla, M.; Balas, F.; Manzano, M.; Vallet-Regí, M. *Chem. Mater.* **2007**, *19*, 3099–3101.
(49) García, A.; Colilla, M.; Izquierdo-Barba, I.; Vallet-Regí, M. *Chem. Mater.* **2009**, *21*, 4135–4145.

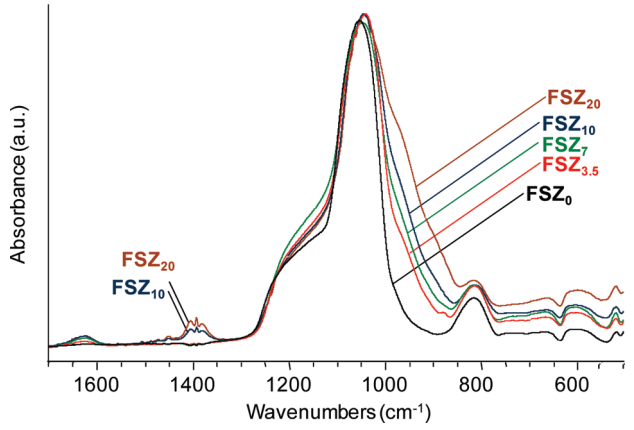

Figure 4. FTIR spectra of FSZ_x materials in the 1700−500 cm^{-1} range.

Table 3. Different Weight Percentages of FSZ_x Materials Calculated Using XRF and EDS

	XRF		EDS	
sample	% SiO_2	% ZrO_2	% SiO_2	% ZrO_2
FSZ_0	99.7	0	100	0
$FSZ_{3.5}$	96.8	2.8	96.9	3.1
FSZ_7	93.8	5.7	94.0	6.0
FSZ_{10}	91.7	7.6	91.0	8.1
FSZ_{20}	80.2	19.1	79.7	20.3

indicate that there is not a clear trend in the t_{wall} with the increase in the ZrO_2 content, being in all cases within the 5.6 to 6.8 range.

The modification of the silica mesostructure with different amounts of zirconia was confirmed by Fourier Transformed Infrared (FTIR) spectroscopy (Figure 4). Typical vibration bands of SiO_2 matrices were observed at ca. 820 cm^{-1} (Si−O symmetric stretching), at ca. 1050 cm^{-1} (Si−O−Si asymmetric stretching) and at ca. 3300 cm^{-1} (O−H stretching from Si−OH groups). ZrO_2 possess strong FTIR adsorption at ca. 800 cm^{-1} due to the ionic character of the Zr−O bonds,[50] but in the case of the binary oxides here produced this band was masked by the Si−O−Si symmetric bond stretching vibration which commonly appears at ca. 800 cm^{-1}. Despite this, there was an increasing shoulder at ca. 950 cm^{-1} as the Zr precursor content was increased as it can be observed in Figure 4. It has been reported previously that zirconium containing silicates show an infrared band at 945−960 cm^{-1}, attributed to the asymmetric stretching vibration of the Si−O−Zr group.[51] Thus, it can be assumed that the zirconium precursor added to the initial solution was acting as a network modifier of the mesostructure and no phase separation between silica and zirconia was observed. The presence of zirconium in the network was also confirmed by XRF and EDS. Both techniques were in good agreement, as it can be observed in Table 3, which proves that the Si/Zr ratio of the oxide formed can be easily controlled by the composition of the reacting mixture. To further evaluate the effect of Zr incorporation into

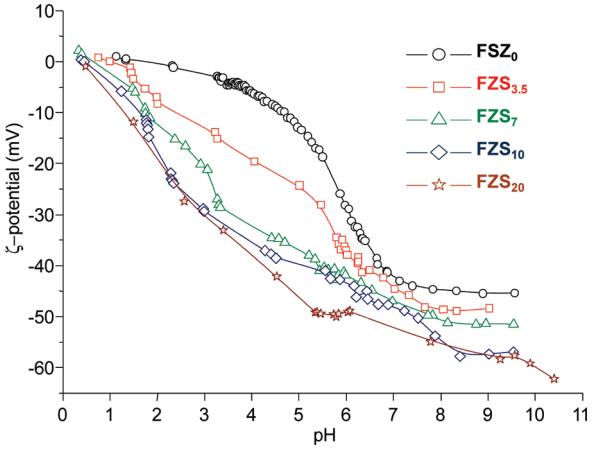

Figure 5. ζ-potential measurements vs pH of FSZ_x materials.

the silica network, ζ-potential measurements versus pH for FSZ_x materials were performed (Figure 5). It can be observed that there is a shift of the isoelectric point (IEP) toward more acidic pH values with the increase in the Zr content. Therefore, the IEP ranges from 1.7 for FSZ_0 to 0.4 for FSZ_{20} materials. These data indicate that Zr incorporation increases the Brönsted acid character of silica, which clearly supports that there is no phase separation between silica and zirconia and that Zr is forming part of the silica network. Otherwise, the IEP of mixed FSZ_x materials would reach an intermediate value between that of pure SiO_2 (2.1) and that of pure ZrO_2 (4.1), as reported in the literature for SBA-15 mesoporous silica partially covered by ZrO_2, which exhibited an IEP of 3.5.[52] It can be observed that there is a shift of the isoelectric point (IEP) toward more acidic pH values with the increase in the Zr content. Therefore, the IEP ranges from 1.9 for FSZ_0 to 0.4 for FSZ_{20} materials (Table 2). These results indicate that Zr addition increases the Brönsted acid character of silica.

It is well-known that the presence of Zr^{4+} tetrahedrally incorporated in the silica network originates Lewis acid centers able to accept electrons from any possible adsorbed molecule.[53] It has been also demonstrated that mixed SiO_2−ZrO_2 oxides have both Lewis and Brönsted acid sites.[46] The understanding of the chemical nature of the surface of the FSZ_x materials is of special interest when these mixed mesoporous oxides are intended as host matrices to adsorb and release biologically active molecules.

In Vitro Bisphosphonates Delivery Tests. The loading of bisphosphonates was carried out with two different drugs that act inhibiting bone resorption by osteoclasts: alendronate and zoledronate. The same phosphonate heads and different chemical tails of these drugs allowed us to establish how the different hydrophobicity affected the adsorption and release kinetics (Figure 6).

XRF measurements were used to quantify the amount of bisphosphonate loading under different conditions, as Figure 7 shows. As a general trend, and with the exception

(50) Wachs, I. E. *Catal. Today* **1996**, *27*, 437–455.
(51) Dang, Z.; Anderson, B. G.; Amenomiya, Y.; Morrow, B. A. *J. Phys. Chem.* **1995**, *99*, 14437–14443.
(52) Gutiérrez, O. Y.; Pérez, F.; Fuentes, G. A.; Bokhimi, X.; Klimova, T. *Catal. Today* **2008**, *130*, 292–301.
(53) Ramanathan, A.; Villalobos, M. C. C.; Kwakernaak, C.; Telalovic, S.; Hanefeld, U. *Chem.—Eur. J.* **2008**, *14*, 961–972.

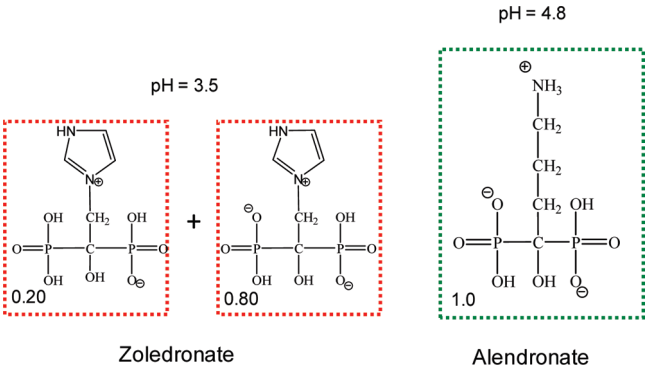

Figure 6. Zoledronate species at their relative abundance at pH 3.5 (left) and alendronate species at their relative abundance at pH 4.8 (right).

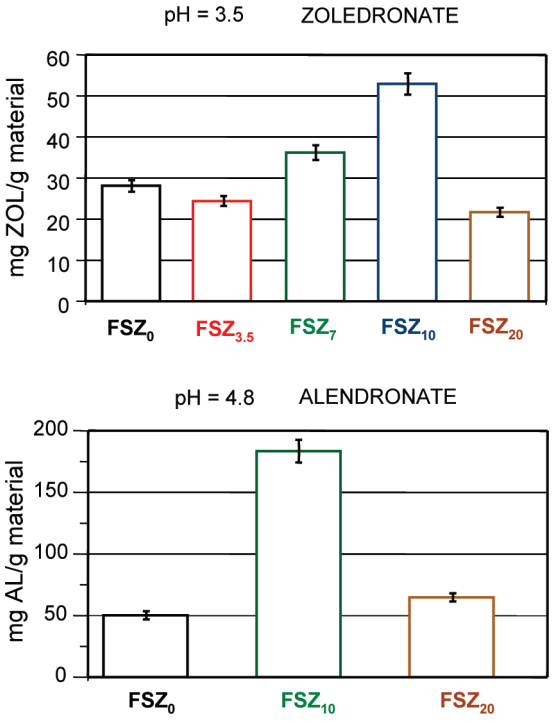

Figure 7. Zoledronate (up) and alendronate (down) loads and the corresponding error bars into different FSZ_x ordered mesoporous binary oxides measured using XRF.

of FZS_{20} as explained before, it was observed that when increasing the amount of zirconium in the silica matrix, there was an enlargement of the amount of drug intake, independently of the drug adsorbed. This effect was attributed to the complexation of the phosphonates from the drug with the zirconia present in the matrix. Zirconium itself is known to be susceptible to nucleophilic reactions, especially when it is bonded to oxygen, and therefore phosphonate groups would tend to be attracted by zirconium species at the surface of the matrix mesopores. In fact, it has been known for decades that phosphates and phosphonates easily react with zirconium oxide networks.[54] This type of complexation has even been used to covalently modify the surface of zirconia particles using phosphated organic species.[55]

However, the different chemical structure at the amine ends of bisphosphonates, alendronate and zoledronate, provoked a different loading behavior. The surface of the mesopores is composed of Si−OH and Zr−OH groups, which provides the surface of a hydrophilic environment that would have an effect over the adsorption of molecules. The amino function present in alendronate provides this drug of hydrophilic character, which promotes higher loading. On the other hand, the imidazole group present in zoledronate provides this drug of hydrophobic character, which promotes a lower degree of loading. Thus, the choice of bisphosphonate to be used in these drug delivery systems would depend on the final requirements in terms of amount of drug needed into the matrix.

The release of both bisphosphonates showed diverse profiles attributable to the different chemical structure of those drugs: alendronate presents a primary amine while zoledronate possesses an imidazole ring. Figure 8 shows the release profiles of alendronate from pure silica material (FSZ_0) and silica-zirconia mesostructured matrices (FSZ_{10} and FSZ_{20}). There is a palpable difference attending to these profiles. When the matrix consists in pure silica, 100% of the alendronate loaded is fully released in ca. 100 h of essay. However, when zirconia is present in the mesostructure, there is a partial retention of the bisphosphonate, and at ca. 100 h of experiment no more than 20% of alendronate loaded has been released. This effect is even more noticeable in the case of FSZ_{10} material which presented the highest drug load and at ca. 100 h the release was lower than 4%. This is an evidence of the complexation that takes place between Zr and phosphates and that has been mentioned above. This attracting interaction provokes a partial retention of the bisphosphonate into the mesostructure. Thus, modulation of the drug release has been achieved through the modification of the matrix with different amounts of Zr, which was one of the aims of this work.

The release of zoledronate, shown in Figure 9, follows a different profile than alendronate. When pure silica matrices (FSZ_0) are used similar type of release curves than those of alendronate are observed. However, when Zr is present into the mesostructure, the release of zoledronate follows a sigmoidal profile composed of three phases: lag phase, burst phase, and saturation phase.[56] This type of profile, also known as the variable slope sigmoid,[57] corresponds to an empirical model described by the Hill equation (eq 1), which is used for many processes that are driven by two different mechanisms: diffusion and chemical reaction

$$\left(\frac{W_t}{W_0}\right) = \left(\frac{W_t}{W_0}\right)_{lag} + \frac{(W_t/W_0)_{max}}{1+(t_{1/2}/t)^H} \qquad (1)$$

(54) Alberti, G.; Torracca, E. J. *Inorg. Nucl. Chem.* **1968**, *30*, 317–318.
(55) Carriere, D.; Moreau, M.; Barboux, P.; Boilot, J. P.; Spalla, O. *Langmuir* **2004**, *20*, 3449–3455.
(56) Cheng, K.; Landry, C. C. *J. Am. Chem. Soc.* **2007**, *129*, 9674–9685.
(57) Giraldo, J.; Vivas, N. M.; Vila, E.; Badia, A. *Pharmacol. Ther.* **2002**, *95*, 21–45.

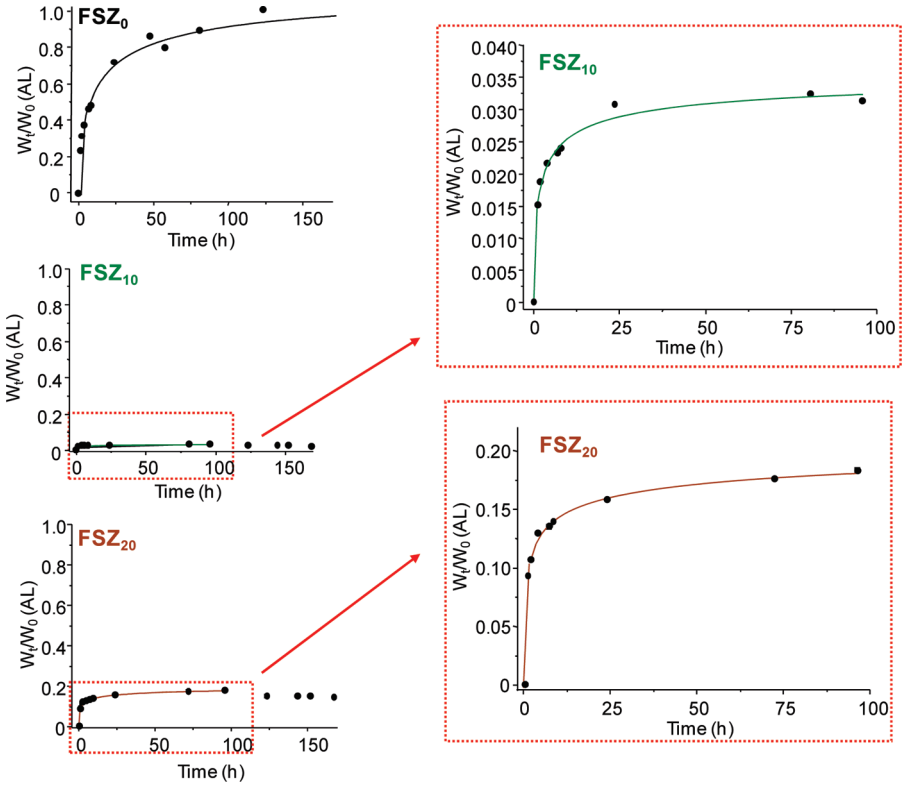

Figure 8. Alendronate (AL) release profiles from different FSZ_x materials.

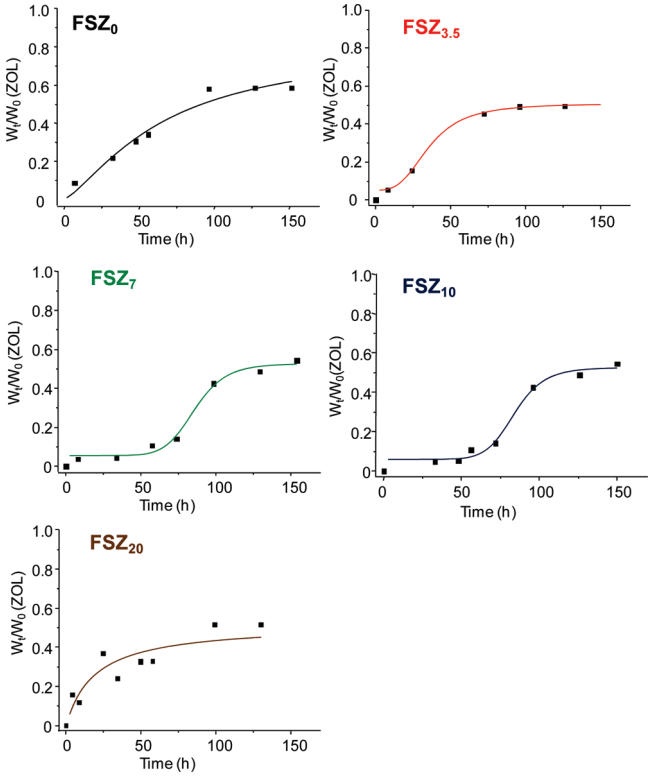

Figure 9. Zoledronate (ZOL) release profiles from FSZ_x materials.

where (W_t/W_0) is the cumulative amount of drug released at time t, $(W_t/W_0)_{lag}$ is the amount of drug released in the lag time, $(W_t/W_0)_{max}$ is the maximum amount of drug released, $t_{1/2}$ is the time at which (W_t/W_0) reaches $(W_t/W_0)_{max/2}$, and H is the Hill coefficient which gives the slope of the sigmoidal curve at $t_{1/2}$. Taking into account that this is an empirical model used to find the mathematical equation that best fits experimental data, which means that equation parameters lack physical meaning, this variable slope sigmoid model is informing us that two processes are taking place during the release of the drug. An initial step, called lag phase, whose length depends on the intrinsic characteristics of the reaction between the drug and the matrix, followed by a diffusion step, where the drug is coming out of the pores.

Tables 4 and 5 show the kinetic release parameters for alendronate and zoledronate from different FSZ_x materials after applying the Hill equation to the obtained delivery profiles. Although this empirical model allows explaining and comparing the undergoing release process from all FSZ_x matrices, it should be mentioned that the quality of the fits is not very high in some cases. In the case of alendronate, the lag phase does not exist, and this explains why the profile is composed of only of burst and saturation phases. The nonexistence of a lag phase could be due to the absence of any reaction between the drug and the matrix, there is only a complexation that retains the drug into the matrix. However, in the case of zoledronate, this lag phase is quite palpable in the plots of $FZS_{3.5}$, FZS_7, and FZS_{10}, Figure 9, and the parameter $(W_t/W_0)_{lag}$ also increases as the zirconium content increases (Table 5). This fact could be explained as follows: the more zirconia in the mesostructure, the more zoledronate adsorbed (as it has been explained before). Therefore, the more zoledronate loaded, the more hydrophobic is the porous environment (as a

Table 4. Kinetic Release Parameters for Alendronate Release from FSZ_x Materials

sample	W_0	$(W_t/W_0)_{lag}$	$(W_t/W_0)_{max}$	$t_{1/2}$	H	R^2	χ^2
FSZ_0	50.2	0	1.16 ± 0.17	12.1 ± 4.7	0.617 ± 0.092	0.988	0.00155
FSZ_{10}	183.4	0	0.0366 ± 0.0030	2.02 ± 0.64	0.52 ± 0.11	0.992	1.11×10^{-6}
FSZ_{20}	64.8	0	0.224 ± 0.015	2.16 ± 0.74	0.380 ± 0.049	0.999	5.7×10^{-6}

Table 5. Kinetic Release Parameters for Zoledronate Release from FSZ_x Materials

sample	W_0	$(W_t/W_0)_{lag}$	$(W_t/W_0)_{max}$	$t_{1/2}$	H	R^2	χ^2
FSZ_0	28.1	0 (fixed)	0.814 ± 0.239	65.0 ± 4.1	1.39 ± 0.16	0.98	0.0014
$FSZ_{3.5}$	24.4	0.0511 ± 0.0070	0.455 ± 0.012	35.7 ± 0.012	3.06 ± 0.26	0.9997	0.00004
FSZ_7	36.2	0.053 ± 0.018	0.475 ± 0.032	83.8 ± 3.1	8.35 ± 1.9	0.991	0.0008
FSZ_{10}	52.9	0.059 ± 0.018	0.467 ± 0.031	84.0 ± 2.9	8.81 ± 1.9	0.991	0.00073
FSZ_{20}	21.7	0 (fixed)	0.52 (fixed)	18.8 ± 5.4	0.98 ± 0.28	0.85	0.0052

consequence of the imidazole ring from this drug). This would lead to a lag phase for the aqueous physiological medium to diffuse into the porous cavities, which is the first step in the release process. It is also possible that zoledronate molecules block the entrances of the mesopores, which would impede the solvent to flow inside the mesopores. Only after the release of those blocking drug molecules (lag period), the solvent could diffuse into the pores and the normal release would take place through burst and saturation phases. Therefore, there would be a delay in the release process, which is responsible for the lag phase in the release profiles.

It should be highlighted that the data presented here (loading, kinetics of release) for the sample containing 20% of Zr do not follow what can be expected from a linear evolution of the main result obtained for the samples with 0, 3.5, 7, and 10% of Zr. Clearly, the drugs loads are lower than expected (Figure 7). This takes partly its origin in the 30% lower surface area and the smaller pore size (5.7 nm when other Zr-containing powders exhibit 10−11 nm cavities) of these particles. Indeed, a strong decrease of surface area limits in similar proportion the maximum loading capacity of zoledronate that is adsorbed at the surface of the porous network. In addition, both the higher zirconium content of the inorganic wall and the smaller pore size of this powder exacerbate very likely the hydrophobicity of the surface via a fast complexation of the external part of each particle. The highly complexed (thus hydrophobic) shell inhibits the penetration of zoledronate salt within the porous core of the particles. In the same way than for other compositions, the complexation strength (thus hydrophobic effect) of phosphonate groups is weaker in acidic solution, thus the zoledronate does not block completely the restrictions its narrower porous network and penetrates deeper into the particles.

FZS_{20} pellets obtained from compressed drug loaded powders do not present a good mechanical integrity. Indeed, when introduced in saline solution, the whole pellet disaggregates in a few seconds. This peculiar behavior is likely to find its origin on the higher ZrO_2 content of this powder promoting a high density layer of zoledronate at the surface of particles that makes difficult the formation of a cohesive packing of particles upon powder compaction. This would be in agreement with the previously commented possible blocking effect of pore entrances by zoledronate molecules. For delivery experiment, particle−particle attractive interactions in the pellets are very weak or inexistent (neither significant amount hydrogen nor covalent bonding are available between complexed zoledronate species at such pH). The strongly negative surface charge of the particles in water at pH 7.4 issued from silicon centers (unaffected by zoledronate complexation) promotes a strong electrostatic interparticular repulsion upon immersion and a very fast disaggregation of the pellet in single particles.

Such behavior was not observed in the case of alendronate probably because it presents a more hydrophilic amine end than zoledronate. Moreover, TEM studies of FSZ_{20} after being loaded with zoledronate and after the release process in saline solution show that the mesoporous structures of the microspheres are preserved (Figure 10). These results indicate the high stability of the SiO_2-ZrO_2 mesostructures here prepared.

Zoledronate release curve of FZS_{20} sample (shown in Figure 9) exhibits a specific shape. In this case, no sigmoidal aspect is observed, and the proportion of zoledronate in the solution is quickly becoming constant when about 45% of zoledronate has been released. In this case, the important zoledronate retention may once again be due to the concomitant smaller pore size and higher hydrophobicity of FZS_{20} particles which may hinder the diffusion of water and thus block efficiently the diffusion of zoledronate.

These results evidence that the release patterns of bisphosphonates can be modulated by incorporating different zirconium amounts into the mesoporous silica framework. First, the delay time in drug release obtained for different FSZ_x matrices is an added value for controlled delivery aimed at bone regeneration technologies. Moreover, the partial retention of bisphosphonates into FSZ_x materials ($0 < x < 20$) observed under the in vitro release assays should not represent a drawback for their potential in vivo application. The mineral phase of natural bone consists of hydroxyapatite (HA), which presents very high affinity toward bisphosphonates. In fact, zoledronate and alendronate have been reported as the most potent bisphosphonates with also exhibit more prolonged duration of action compared to

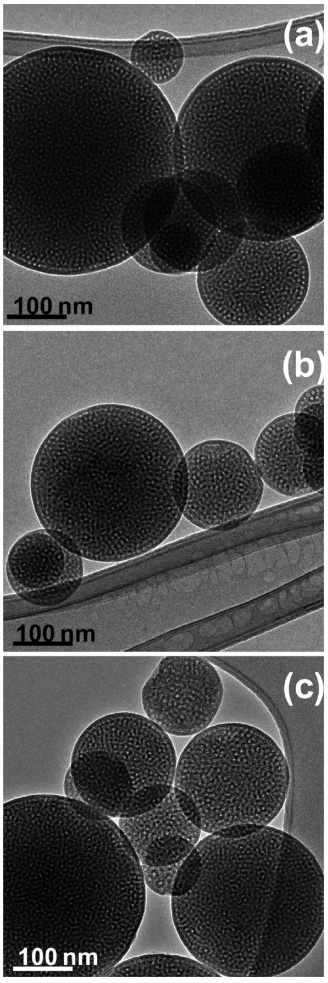

Figure 10. TEM images corresponding to FSZ_{20} sample (a) as synthesized, (b) after being loaded with zoledronate, and (c) after the release process (160 h in the delivery medium).

other employed bisphosphonates.[21,58] This behavior is tightly related to the different binding affinities of HA toward bisphosphonates depending on their chemical nature. Thus, the highest affinity of HA toward alendronate and zoledronate provokes the highest potency, pharmacokinetic, and persistence of effect of these drugs compared to other bisphosphonates.

The actuation mechanisms of bisphosphonates when orally administrated involve that bone skeleton acts as a reservoir of bisphosphonates. This produces drug concentrations in solution at local level near bone cells that are related to the adsorption and desorption properties of bisphosphonates on and off bone surfaces. Therefore, bisphosphonates stored into some of the FSZ_x materials here presented are expected to show high affinity toward HA when in vivo implanted in the cavity of an osteoporotic bone. Otherwise, the silica-zirconia mesoporous material itself would be acting as reservoir of bisphosphonates. In any case, these mixed mesoporous silica-zirconia oxides open promising expectations in the clinical field for the local treatment of bone diseases acting as controlled delivery devices of bisphosphonates.

(58) Nancollas, G. H.; Tang, R.; Phipps, R. J.; Henneman, Z.; Gulde, S.; Wu, W.; Mangood, A.; Russell, R. G. G.; Ebetino, F. H. *Bone* **2006**, *38*, 617–627.
(59) Ravikovitch, P. I.; Neimark, A. V. *Colloids Surf. A* **2001**, *187*, 11–21.

Conclusions

This work presents the possibility of tuning the control release of certain drugs varying the composition of mesostructured binary oxides. It represents the first time that binary ordered mesoporous oxides (silica-zirconia) have been used as drug delivery systems. The loading of different bisphosphonates, alendronate and zoledronate, with similar phosphonate heads and different amine tails in terms of acidity and hydrophobicity has been achieved. Thus, depending on the required drug dosage, a different loading pH will have to be used to modulate the bisphosphonate uptake into these materials.

The selection of the material composition allows controlling the surface properties of the mesoporous matrix, which would tailor the amount of drug adsorbed into the mesopores. The introduction of zirconia into a silica network produces the creation of Lewis acid centers able to accept electrons from the adsorbed molecule. ζ-potential measurements revealed that the zirconia addition increased not only the Lewis but also the Brönsted acid character of silica and that silicon is the main element present on the surface of the materials.

Finally, the modification of silica ordered mesoporous materials with zirconia, even in low concentration, produces a noticeable modification on the release of bisphosphonates. There is a partial retention of the drug because of the complexation of the phosphonates from the drug with the zirconia present in the matrix, which leads to a more sustained release of the drug. These binary ordered mesoporous oxides act as controlled release vectors of bisphosphonates. Thus, processing powders with variable percentages of pure SiO_2 and a mixed zirconium oxide such as FZS_{10} would allow a very fine control of the drug dosage. This opens the possibility of designing drug carriers with different adsorption capacities and also different release kinetics. The choice would depend on the amount of drug required for each biomedical application.

Acknowledgment. We thank the following for funding this work: the Spanish CICYT through projects MAT2008-00736 and the Comunidad Autónoma de Madrid via the S2009MAT-1472 program grant. Functionalized Advanced Materials and Engineering (FAME) European Network of Excellence is also acknowledged.